Monocytic myeloid-derived suppressor cells home to tumor-draining lymph nodes via CCR2 and locally modulate the immune response

Lahmar, Qods; Schouppe, Elio; Morias, Yannick; Van Overmeire, Eva; De Baetselier, Patrick; Movahedi, Kiavash; Laoui, Damya; Sarukhan, Adelaida; Van Ginderachter, Jo A

Published in:
Cellular Immunology

DOI:
10.1016/j.cellimm.2021.104296

Publication date:
2021

Monocytic myeloid-derived suppressor cells home to tumor-draining lymph nodes via CCR2 and locally modulate the immune response.

Qods Lahmar[1,2,+], Elio Schouppe[1,2,+], Yannick Morias[1,2], Eva Van Overmeire[1,2], Patrick De Baetselier[1,2], Kiavash Movahedi[1,2], Damya Laoui[1,2], Adelaida Sarukhan[1,2,3,*], and Jo A. Van Ginderachter[1,2,*]

[1]Myeloid Cell Immunology Lab, VIB Center for Inflammation Research, Brussels, Belgium
[2]Laboratory of Cellular and Molecular Immunology, Vrije Universiteit Brussel, Brussels, Belgium
[3]INSERM, 101 rue Tolbiac, Paris 75013, France
[+]These authors contributed equally to this work
*These authors contributed equally to this work

Running title: Role of MO-MDSC in tumor draining LN.

Keywords: MO-MDSC, Tumor-draining lymph node, CCR2

Financial support:
This work was supported by a doctoral grant from FWO-Vlaanderen to E.S., E.V.O., and K.M., a scholarship from "Stichting Emmanuel van der Schueren" to E.S., D.L., and K.M., a doctoral grant from IWT-Vlaanderen to D.L., and Y.M., and a grant from "Stichting tegen Kanker" to P.D.B. and J.A.V.G.. A.S. received financial support from INSERM. This work was also part of the COST Action BM1404 Mye-EUNITER (www.mye-euniter.eu<http://www.mye-euniter.eu>), supported by COST (European Cooperation in Science and Technology). COST is part of the EU Framework Programme Horizon 2020.

Corresponding author:
Dr. Jo A. Van Ginderachter, Lab of Cellular and Molecular Immunology, Vrije Universiteit Brussel, VIB Center for Inflammation Research, Building E8, Pleinlaan 2, B-1050 Brussels, Belgium. E-mail: jo.van.ginderachter@vub.be.

The authors have no conflicting financial interests.

Word count: 2379
Table count: 0
Figure count: 4

List of abbreviations:
cLN = contralateral lymph node
DC = dendritic cell
MO-MDSC: monocytic myeloid-derived suppressor cell
PMN-MDSC: polymorphonuclear myeloid-derived suppressor cell
TB = tumor-bearing
tdLN = tumor-draining lymph node

Abstract

Efficient priming of anti-tumor T cells requires the uptake and presentation of tumor antigens by immunogenic dendritic cells (DCs) and occurs mainly in lymph nodes draining the tumor (tdLNs). However, tumors expand and activate myeloid-derived suppressor cells (MDSCs) that inhibit CTL functions by several mechanisms. While the immune-suppressive nature of the tumor microenvironment is largely documented, it is not known whether similar immune-suppressive mechanisms operate in the tdLNs. In this study, we analyzed MDSC characteristics within tdLNs. We show that, in a metastasis-free context, MO-MDSCs are the dominant MDSC population within tdLNs, that they are highly suppressive and that tumor proximity enhances their recruitment to tdLN via a CCR2/CCL2-dependent pathway. Altogether our results uncover a mechanism by which tumors evade the immune system that involves MDSC-mediated recruitment to the tdLN and the inhibition of T-cell activation even before reaching the highly immunosuppressive tumor microenvironment.

Introduction

Seminal studies in several solid tumor types indicated that the presence of Th1/CTL gene signatures in the tumor microenvironment are the strongest prognostic factors for recurrence and overall survival (1). Priming of these cells is typically confined to the tumor-draining lymph nodes (tdLNs) (2,3), although it may occur as well in intratumoral tertiary lymphoid organ structures (4, 5). Nevertheless, activated CTLs rarely cause tumor rejection, mainly due to the immunosuppressive/tolerogenic nature of the tumor microenvironment (2, 6). However, whether similar immunosuppressive mechanisms are at play in the tdLNs remains poorly explored.

In this respect, tumors are known to expand and activate myeloid-derived suppressor cells (MDSCs), which hamper T-cell functions in a variety of pathologies (7, 8). These cells originate from bone marrow progenitors during "emergency" hematopoiesis driven by hematopoietic growth factors and inflammatory mediators (9). MDSCs comprise an immature monocytic $CD11b^{+}CD115^{+}Ly6G^{-}Ly6C^{high}$ (MO-MDSC) and granulocytic $CD11b^{+}CD115^{-}Ly6G^{+}Ly6C^{int}$ (PMN-MDSC) population (10). MO-MDSCs require IFN-γ stimulation and NO production to inhibit T-cell functions (11), while PMN-MDSCs mostly employ reactive oxygen/nitrogen species that nitrate and disable TCR and CD8 molecules (12). In addition, MDSCs lower the availability of L-arginine and cysteine, both of which are essential amino acids for T-cell activation (7,13,14). Remarkably, MDSC activity has mainly been studied in tumor and spleen, but their presence and function at the site where the actual T-cell priming occurs, the tdLN, has poorly been investigated.

Here, we explored the presence and the type of MDSC within tdLNs that were not affected by metastases. We show that, in contrast to spleen or bone marrow, MO-MDSCs are the predominant population in tdLNs due to CCR2-mediated migration and that they have a potent immunosuppressive potential.

Material and Methods

Mice

Six-week-old female CD45.2 and CD45.1 C57BL/6 mice were from Janvier (St Berthevin Cedex, France). Six-week-old female CD45.2 Ubiquitin-GFP (Ubi-GFP) C57BL/6 mice were from Jackson Laboratories (Bar Harbor, ME, USA). CD45.2 CCR2$^{-/-}$ and OT-I TCR transgenic C57BL/6 mice were provided by Frank Tacke (Aachen University, Germany), and Karine Breckpot (VUB, Belgium), respectively. Procedures followed the guidelines of the Belgian Council for Laboratory Animal Science.

Cell lines, tumor growth

EG7-OVA (ovalbumin-transfected EL-4 thymoma), E0771 mammary carcinoma and 3LL-R Lewis Lung carcinoma (15) cells were cultured in RPMI with 10% FCS, 0.03% L-glutamine, 100 µg/mL streptomycin, 100 U/mL penicillin (Invitrogen, Carslbad, CA, USA). For MDSC - OT-1 splenocyte co-cultures, this medium was further supplemented with 1 mM nonessential amino acids, 1 mM sodium pyruvate (Invitrogen), and 0.02 mM 2-mercaptoethanol. Mice were injected subcutaneously with 3x10^6 cancer cells.

Cell Isolation

Splenic MO- and PMN-MDSCs were purified from the spleen of tumor-bearers as described (10,11). To purify lymph node- and spleen-associated MDSC subsets and in one experiment, brachial, axillary LNs and spleen were collected, depleted from red blood cells, CD11b$^+$ cells were enriched magnetically (anti-CD11b microbeads, Miltenyi Biotec) followed by sorting of MO- and PMN-MDSCs using a BD FACSAria II (BD Biosciences). To purify bone marrow-associated CD11b$^+$ cells, the tibiae and femurs were collected and flushed. After red blood cell-depletion, CD11b$^+$ cells were purified via magnetic selection (anti-CD11b microbeads, Miltenyi Biotec). To assess MDSC presence in EG7-OVA tumors, surgically removed tumors were enzymatically digested to prepare a tumor single cell suspension as previously described (15), however without performing a density gradient (usually done to remove dead cells and debris) not to alter the MO-/PMN-MDSC ratio.

Flow cytometry

Antibodies used in this study are listed in Supplementary Table 1. To block Fc receptors, cells were pre-incubated on ice with anti–mouse CD16/CD32 (clone 2.4G2). Data were acquired on a FACS Canto II (BD Bioscience) and analyzed by FlowJo software version 9.3.2 (Tree Star, Ashland, OR, USA).

OT-I T-cell suppression

Splenic MO-MDSCs were added in various amounts to $2x10^5$ OT-I splenocytes in flat-bottomed 96-well plates and stimulated with 250 μg/mL ovalbumin (Sigma-Aldrich). After 24 h, 1 μCi ^{3}H-thymidine (Amersham Biosciences Ltd, Bucks, UK) was added to the co-culture and cells were allowed to proliferate for another 18 h before counts-per-minute measurement on a Wallac 1450 Liquid Scintillation Counter.

NO_2^- quantification

NO_2^- was measured as described (10).

BrdU incorporation

Mice were given two i.p. injections of 1 mg BrdU (Sigma-Aldrich) within a two-hour interval. Six hours after the initial BrdU pulse, intracellular BrdU staining was performed using the BrdU Flow kit (BD Bioscience).

MDSC adoptive transfer

Bone marrow $CD11b^+$ cells from EG7-OVA tumor-bearing Ubi-GFP CD45.2 mice were i.v. injected ($5\text{-}7x10^6$) in naïve or EG7-OVA tumor-bearing CD45.1 mice. Alternatively, these cells were mixed (1/1 ratio) with bone marrow $CD11b^+$ cells from EG7-OVA tumor-bearing $CCR2^{-/-}$ mice and $5\text{-}7x10^6$ of each population was injected. 1 day later, spleen, draining brachial and axillary lymph nodes, and contralateral brachial and axillary lymph nodes were collected and analyzed for the presence of transferred MDSCs.

Splenectomy

For splenectomy, the abdomen was opened under general anesthesia, spleen vessels were cauterized and the spleen was carefully removed. As sham surgery, the abdomen was opened but the spleen was not removed. Two weeks later, mice were injected with EG7-OVA.

CCL2 ELISA

LN were weighed, resuspended in 250 µl 1X protease inhibitor buffer (Roche), teased into pieces and sonicated, followed by centrifugation (13000 rpm, 20 min, 4°C), and supernatant collection. CCL2 was measured via ELISA (R&D systems).

Real‐time quantitative reverse transcription PCR (qRT‐PCR)

These experiments were performed as described before [15]. The primers are listed in Supplementary Table 2.

Statistical Analysis

Statistical significance was determined by the Mann-Whitney test or Wilcoxon matched pairs test, using Prism 4.0 software (GraphPad Software, San Diego, CA, USA).

Results

MO-MDSCs, but not PMN-MDSCs, accumulate in tumor-draining lymph nodes.

It is well established that in tumor-bearing (TB) animals PMN-MDSCs are often the most prominent MDSC subset, at least in the spleen (10). However, less is known about the MDSC distribution in the lymph nodes. In order to address this issue, we investigated the MDSC composition in the spleen (SPL), the contra-lateral lymph nodes (cLN) and the tumor draining lymph nodes (tdLN) of 21 days EG7-OVA TB mice. Interestingly, while $CD11c^{-}CD11b^{+}Ly6G^{+}Ly6C^{int}$ PMN-MDSCs were indeed more abundant than $CD11c^{-}CD11b^{+}Ly6G^{-}Ly6C^{hi}$ MO-MDSCs in the spleen, this ratio was completely inverted in the cLN and especially the tdLN (Figure 1A; gating strategy Supplementary Figure 1). In terms of absolute numbers, tdLNs contained significantly more MO-MDSCs than the cLNs in the same mice, suggesting that tumor proximity favored MO-MDSC accumulation in the lymph nodes (Figure 1B). Notably, these LN-infiltrating MO-MDSCs do not seem to originate from the spleen, which may function as a reservoir for monocytes (16, 17), since the numbers of tdLN-associated MO-MDSCs and the MO-/PMN-MDSC ratio were not significantly altered in splenectomized mice (Figure 1C-D). Finally, similar observations were made with other experimental models of cancer: tdLNs from subcutaneous 3LL-R lung carcinoma and E0771 mammary carcinoma tumors (Supplementary Figure 2), also showed increased numbers of MO-MDSC and an increased MO-/PMN-MDSC ratio.

To ascertain that the $CD11b^{+}Ly6G^{-}Ly6C^{hi}$ cells from tdLNs were *bona fide* MO-MDSCs, these cells were sorted and their capacity to suppress $CD8^{+}$ T cell proliferation was tested *in vitro*. Notably, MO-MDSCs isolated from tdLNs displayed a higher suppressive capacity as compared to their splenic counterparts (Figure 1E). In accordance, they also produced higher levels of NO (Figure 1F), which is the main T-cell suppressive mechanism employed by these cells (10,11).

Accumulation of MO-MDSCs in tdLNs is due to preferential homing and not to *in situ* proliferation

The inverted MO-/PMN-MDSC ratio in tdLNs could be due to preferential homing of monocytic cells to that site, to their *in situ* proliferation, or to their enhanced survival in

the LNs. *In vivo* pulse labeling with BrdU did not reveal a significant level of MO- nor PMN-MDSC proliferation in the LNs, whereas a subpopulation of MO-MDSCs actively divides in the spleen (Figure 2A). Furthermore, AnnexinV staining did not indicate enhanced PMN-MDSC apoptosis in the LN (data not shown). In order to address the homing capacities of PMN- and MO-MDSCs, we adoptively transferred total $CD11b^+$ cells (encompassing $CD11b^+Ly6G^-Ly6C^{hi}$ monocytic and $CD11b^+Ly6G^+Ly6C^{int}$ granulocytic cells at a known ratio) from the bone marrow of TB Ubi-GFP transgenic mice into non-transgenic naïve and TB recipients (Figure 2B). 14-16h after transfer, the ratio of GFP^+ MO- and PMN-MDSCs was analyzed in the bone marrow, spleen and lymph nodes of the recipients and compared to the ratio in the originally transferred population. Remarkably, in naïve mice, the PMN-MDSC subset was over-represented (reduced MO-/PMN-MDSC ratio compared to the transferred population) in both spleen and LNs, a feature that is maintained in the spleen of TB mice (Figure 2C-D). In contrast, MO-MDSCs became over-represented (increased MO-/PMN-MDSC ratio compared to the transferred population) in tdLNs. These results show for the first time that, despite the inherently better migratory capacity of PMN-MDSCs to spleen and LN (as observed in naïve mice), preferential MO-MDSC homing to LNs is enhanced by tumor proximity.

Presence of MO-MDSCs in the tdLN is not due to cancer cell metastasis

It could be argued that, after a prolonged period of primary tumor growth, the tdLN is colonized by metastatic cells whereby the MDSC ratio merely mirrors the situation in the primary tumor. However, this hypothesis is refuted by the observation that PMN-MDSC outnumber MO-MDSC within EG7-OVA tumors after 21 days of tumor growth (Figure 3A), while the inverse situation is true in the tdLN (Figure 1A). The same holds true for 3LL-R tumors after 19 days of tumor growth (Supplementary Figure 2A, Supplementary Figure 3). To formally exclude the possibility that the preferential MO-MDSC homing to tdLNs is driven by cancer cell metastasis, we analyzed spleen and LNs in an earlier time frame, ranging between 5 and 10 days after EG7-OVA tumor inoculation. First, we measured OVA mRNA presence by RT-PCR in the different organs after 5, 7 and 10 days of tumor progression. While the primary tumor exhibited a high level of OVA expression, OVA mRNA was undetectable in the spleen, cLN and tdLN at least until day 10 (Figure 3B), indicating that no metastasis occurred in these organs. Analysis of the MDSC composition at these early time points confirmed that by day 10, both the MO-/PMN-MDSC ratio and

the total number of MO-MDSC in the tdLN were significantly higher as compared to the cLN (Figure 3C-D). Moreover, adoptive transfer of $CD11b^+$ bone marrow cells from tumor-bearing Ubi-GFP+ mice to 10 day tumor-bearing recipients resulted again in an over-representation of MO-MDSCs in the tdLN as compared to the cLN or to LN of naïve mice (Figure 3E). Thus, the recruitment of MO-MDSC in tdLN occurs in a metastasis-free context and is regulated by a proximal primary tumor.

Homing of MO-MDSCs to tdLNs is CCR2-dependent

Homing of $Ly6C^{hi}$ monocytes to LNs has been shown to depend on CCR2, rather than CCR7, upon viral infection or immunization (18). Interestingly, while CCR7 expression by tdLN-associated MO-MDSCs was relatively low and similar to that of PMN-MDSCs, CCR2 was only strongly expressed by MO-MDSCs (Figure 4A), suggesting a specific role for this chemokine receptor in MO-MDSC behavior. Moreover, CCL2 - as main CCR2 ligand - is present at a higher level in tdLNs than in cLNs, both at day 10 (Supplementary Figure 4) and day 21 of tumor growth (Figure 4B). Strikingly, CCL2 mRNA was only detected in the tumor, but not in the cLN nor in the tdLN (Supplementary Figure 5), suggesting that the CCL2 protein in the tdLN is not produced *in situ* but rather derives from the tumor microenvironment.

In line with a potential MO-MDSC-steering role for CCR2, the preferential homing of MO-MDSCs to tdLNs is largely absent in CCR2-deficient animals and is replaced by a massive influx of PMN-MDSCs (Figure 4C). However, data in these mice are difficult to interpret because monocytes need CCR2 to emigrate from the bone marrow and hence CCR2-deficient animals contain strongly reduced monocyte numbers in their blood (19). To unequivocally test the implication of CCR2 during MO-MDSC migration from the blood to the tdLNs, we intravenously transferred a 1:1 mixture of $CD45.2^+GFP^+$ wild type (WT) and $CD45.2^+$ $GFP^-CCR2^{-/-}$ bone marrow MDSCs into congenic $CD45.1^+$ tumor-bearing recipients (Figure 4D scheme) and analyzed the ratio of $CD45.2^+GFP^+$ (WT)/$CD45.2^+GFP^-$ ($CCR2^{-/-}$) cells in tdLNs and cLNs (Figure 4D lower panel). The homing to LNs was equal between wild type and CCR2-deficient PMN-MDSCs. Conversely, WT MO-MDSCs displayed a competitive advantage over $CCR2^{-/-}$ MO-MDSCs to enter the tdLNs. These data indicate that CCR2 plays an important role in MO-MDSC, but not PMN-MDSC, homing to tumor-draining lymph nodes.

Discussion

In this study, we demonstrated that MO-MDSCs are the dominant MDSC population within lymph nodes and that tumors enhance their recruitment to the draining LN, at least partly through CCR2/CCL2 interactions.

To our knowledge, this one of the first studies that addresses the presence and role of MDSCs in tumor-draining lymph nodes. It had been previously described that the immunological reactivity of tdLN decreases as tumors progress (20), but the role of tumor-induced suppressive cells in these studies was not defined. In another study, the adoptive transfer of total MDSCs induced $CD8^+$ T-cell anergy in peptide vaccine draining lymph nodes (21), although by day 10 all transferred MDSCs had differentiated or died. In addition, the therapeutic effects of tdLN cells from mice reconstituted with $Gr1^+$ MDSCs from TB mice was decreased, suggesting that MDSCs can regulate initiation of antitumor immunity in tdLN by suppressing the generation of tumor-specific T cells (22). Finally, tumors that secrete VEGF-C were shown to trigger lymphatic endothelial cells for the attraction of MDSCs in a CXCR2-dependent fashion (23).

Here, we demonstrate that the number of MDSCs is significantly increased within draining LNs of TB mice and that MO-MDSCs are the dominant population, in contrast to the PMN-MDSC dominance observed in the spleen. Furthermore, MO-MDSC homing to the LNs required the chemokine receptor CCR2 and was greatly enhanced by tumor proximity in the absence of LN metastasis. The precise mechanisms by which the tumor favors $CCR2^{hi}$ MO-MDSC cell recruitment to the draining LNs remain to be determined. Our data show a higher level of the CCL2 protein in tdLN as compared to cLN (Figure 4B), while CCL2 mRNA was undetectable in these organs in comparison to the tumor site (Supplementary Figure 5). These results thus strongly suggest that CCL2 produced in the tumor could be transported via the lymph to HEVs in the draining lymph nodes as described for inflamed skin (24). In addition, tumor-derived exosomes have been shown to reach the draining LNs (25), and melanoma- and colorectal carcinoma-derived exosomes have been reported to alter monocyte differentiation into DCs, leading to the generation of MDSCs (26). Alternatively, it can not be formally excluded that tdLN MO-MDSCs first underwent a passage in the TME before migrating to the tdLN. The eventual contribution of these phenomena to the recruitment and/or in situ generation of the MO-MDSC population in

the tdLNs remain to be explored. In any case, interfering with the CCL2-CCR2 axis has been assessed as a therapeutic option in cancer, because $CCR2^+$ monocytes have also been reported to generate tumor-promoting macrophages (15) and dendritic cells (27) within primary tumors, and metastasis-associated macrophages at the metastatic site (28). Of note, a cessation of the therapy may lead to a massive rebound release of monocytes from the bone marrow, and consequently accelerate metastasis formation (29).

Splenic MO-MDSCs have been shown to play an active role in inducing tumor-specific $CD8^+$ T-cell tolerance by altering the marginal zone architecture in the spleen, and their removal by splenectomy improves tumor responses (30). Our splenectomy experiments demonstrate that tdLN MO-MDSCs are not derived from the splenic reservoir and suggest that they may contribute non-redundantly to tumor-specific tolerance. In fact, MO-MDSCs from tdLN proved more potent in suppressing T cell responses than their splenic counterparts, suggesting that, even though at low frequencies, LN-associated MO-MDSCs could play a major role in suppressing T cell responses *in situ*. Our findings confirm the notion that MDSCs differ in suppressive capacity depending on their location and suggest the establishment of a spleen < tdLN < tumor gradient in terms of suppressive capacity, depending very likely on environmental cues such as the degree of inflammation.

A multitude of strategies has been proposed to target MDSCs and enhance anti-tumor immunity (31). Several of these therapeutic approaches aim to reduce the presence or suppressive capacity of MDSCs in the TME, with often a particular focus on PMN-MDSCs. Our findings suggest that such approaches may not be sufficient to affect the immunosuppressive capacity of MO-MDSCs in the tdLN. Since the tdLN is considered to be an important site for the induction of anti-tumor immune responses, future MDSC-targeted therapies should try to interfere with MO-MDSCs at this site, whereby a blockade of the CCL2-CCR2 axis could be an interesting option.

ACKNOWLEDGEMENTS

The authors thank Ella Omasta, Marie-Thérèse Detobel, Maria Slazak, Yvon Elkrim and Lea Brys for excellent animal care and technical assistance, Nadia Abou and Eddy Vercauteren for administrative assistance, Dr. Carl De Trez and Dr. Benoit Stijlemans for advice and helpful suggestions.

References

1. J Galon, HK Angell, D Bedognetti, FM Marincola, The continuum of cancer immunosurveillance: prognostic, predictive, and mechanistic signatures, Immunity 39 (2013) 11–26.

2. JJ Engelhardt, B Boldajipour, P Beemiller, P Pandurangi, C Sorensen, Z Werb, M Egeblad, MF Krummel, Marginating dendritic cells of the tumor microenvironment cross-present tumor antigens and stably engage tumor-specific T cells, Cancer Cell 21 (2012) 402–417.

3. EJ Villablanca, L Raccosta, D Zhou, R Fontana, D Maggioni, A Negro, F Sanvito, M Ponzoni, B Valentinis, M Bregni, et al, Tumor-mediated liver X receptor-alpha activation inhibits CC chemokine receptor-7 expression on dendritic cells and dampens antitumor responses, Nat Med 16 (2010) 98–105.

4. L De Chaisemartin, J Goc, D Damotte, P Validire, P Magdeleinat, M Alifano, I Cremer, WH Fridman, C Sautès-Fridman, MC Dieu-Nosjean, Characterization of chemokines and adhesion molecules associated with T cell presence in tertiary lymphoid structures in human lung cancer, Cancer Res 71 (2011) 6391–6399.

5. C Sautès-Fridman, F Petitprez, J Calderaro, WH Fridman, Tertiary lymphoid structures in the era of cancer immunotherapy, Nat Rev Cancer 19 (2019) 307-325.

6. E Schouppe, P De Baetselier, JA Van Ginderachter, A Sarukhan, Instruction of myeloid cells by the tumor microenvironment: Open questions on the dynamics and plasticity of different tumor-associated myeloid cell populations, Oncoimmunol 1 (2012) 1135-1145.

7. DI Gabrilovich, S Ostrand-Rosenberg, V Bronte, Coordinated regulation of myeloid cells by tumours, Nat Rev Immunol 12 (2012) 253–268.

8. G Pawelec, CP Verschoor, S Ostrand-Rosenberg, Myeloid-derived suppressor cells: not only in tumor immunity, Front Immunol 10 (2019) 1099.

9. I Marigo, E Bosio, S Solito, C Mesa, A Fernandez, L Dolcetti, S Ugel, N Sonda, S Bicciato, E Falisi, et al, Tumor-induced tolerance and immune suppression depend on the C/EBPbeta transcription factor, Immunity 32 (2010) 790–802.

10. K Movahedi, M Guilliams, J Van den Bossche, R Van den Bergh, C Gysemans, A Beschin, P De Baetselier, JA Van Ginderachter, Identification of discrete tumor-induced myeloid-derived suppressor cell subpopulations with distinct T cell-suppressive activity, Blood 111 (2008) 4233–4244.

11. E Schouppe, C Mommer, K Movahedi, D Laoui, Y Morias, C Gysemans, A Luyckx, P De Baetselier, JA Van Ginderachter, Tumor-induced myeloid-derived suppressor cell subsets exert either inhibitory or stimulatory effects on distinct CD8+ T-cell activation events, Eur J Immunol 43 (2013) 2930–2942.

12. S Nagaraj, K Gupta, V Pisarev, L Kinarsky, S Sherman, L Kang, DL Herber, J Schneck, DI Gabrilovich, Altered recognition of antigen is a mechanism of CD8+ T cell tolerance in cancer, Nat Med 13 (2007) 828–835.

13. MK Srivastava, P Sinha, VK Clements, P Rodriguez, S Ostrand-Rosenberg, Myeloid-derived suppressor cells inhibit T-cell activation by depleting cystine and cysteine, Cancer Res 70 (2010) 68–77.

14. G Mondanelli, S Ugel, U Grohmann, V Bronte, The immune regulation in cancer by the amino acid metabolizing enzymes ARG and IDO, Curr Opin Pharmacol 35 (2017) 30-39

15. K Movahedi, D Laoui, C Gysemans, M Baeten, G Stangé, J Van den Bossche, M Mack, D Pipeleers, P In 't Veld, P De Baetselier, et al, Different tumor microenvironments contain functionally distinct subsets of macrophages derived from Ly6C(high) monocytes, Cancer Res 70 (2010) 5728-5739.

16. FK Swirski, M Nahrendorf, M Etzrodt, M Wildgruber, V Cortez-Retamozo, P Panizzi, JL Figueiredo, RH Kohler, A Chudnovskiy, P Waterman, et al, Identification of splenic reservoir monocytes and their deployment to inflammatory sites, Science 325 (2009) 612–606.

17. V Cortez-Retamozo, M Etzrodt, A Newton, PJ Rauch, A Chudnovskiy, C Berger, RJ Ryan, Y Iwamoto, B Marinelli, R Gorbatov, et al, Origins of tumor-associated macrophages and neutrophils, Proc Natl Acad Sci USA 109 (2012)2491-2496.

18. H Nakano, KL Lin, M Yanagita, C Charbonneau, DN Cook, T Kakiuchi, MD Gunn, Blood-derived inflammatory dendritic cells in lymph nodes stimulate acute T helper type 1 immune responses, Nat Immunol 10 (2009) 394–402.

19. NV Serbina, EG Pamer, Monocyte emigration from bone marrow during bacterial infection requires signals mediated by chemokine receptor CCR2, Nat Immunol 7 (2006) 311–317.

20. KM Hargadon, CC Brinkman, SL Sheasley-O'neill, LA Nichols, TNJ Bullock, VH Engelhard, Incomplete differentiation of antigen-specific CD8 T cells in tumor-draining lymph nodes, J Immunol 177 (2006) 6081–6090.

21. S Solito, V Bronte, S Mandruzzato, Antigen specificity of immune suppression by myeloid-derived suppressor cells, J Leukoc Biol 90 (2011) 31–36.

22. S Watanabe, K Deguchi, R Zheng, H Tamai, L-X Wang, PA Cohen, S Shu, Tumor-induced CD11b+Gr-1+ myeloid cells suppress T cell sensitization in tumor-draining lymph nodes, J Immunol 181 (2008) 3291–3300.

23. J-Y Chen, Y-S Lai, P-Y Chu, S-H Chan, L-H Wang, W-C Hung, Cancer-Derived VEGF-C Increases Chemokine Production in Lymphatic Endothelial Cells to Promote CXCR2-Dependent Cancer Invasion and MDSC Recruitment, Cancers 11 (2019) 1120

24. RT Palframan, S Jung, G Cheng, W Weninger, Y Luo, M Dorf, DR Littman, BJ Rollins, H Zweerink, A Rot, et al, Inflammatory chemokine transport and presentation in HEV: a remote control mechanism for monocyte recruitment to lymph nodes in inflamed tissues, J Exp Med 194 (2001) 1361–1373.

25. S Rana, K Malinowska, M Zöller, Exosomal tumor microRNA modulates premetastatic organ cells, Neoplasia 15 (2013) 281–295.

26. R Valenti, V Huber, P Filipazzi, L Pilla, G Sovena, A Villa, A Corbelli, S Fais, G Parmiani, L Rivoltini, Human tumor-released microvesicles promote the differentiation of myeloid cells with transforming growth factor-beta-mediated suppressive activity on T lymphocytes, Cancer Res 66 (2006) 9290–9298.

27. D Laoui, J Keirsse, Y Morias, E Van Overmeire, X Geeraerts, Y Elkrim, M Kiss, E Bolli, Q Lahmar, D Sichien, et al, The tumour microenvironment harbours ontogenically distinct dendritic cell populations with opposing effects on tumour immunity, Nat Commun 7 (2016) 13720.

28. BZ Qian, J Li, H Zhang, T Kitamura, J Zhang, LR Campion, EA Kaiser, LA Snyder, JW Pollard, CCL2 recruits inflammatory monocytes to facilitate breast-tumour metastasis, Nature 475 (2011) 222-225.

29. L Bonapace, MM Coissieux, J Wyckoff, KD Mertz, Z Varga, T Junt, M Bentires-Alj, Cessation of CCL2 inhibition accelerates breast cancer metastasis by promoting angiogenesis, Nature 515 (2014) 130-133.

30. V Bronte, MJ Pittet, The spleen in local and systemic regulation of immunity. Immunity, 39 (2013) 806-818.

31. Y Wang, A Jia, Y Bi, Y Wang, Q Yang, Y Cao, Y Li, G Liu, Targeting myeloid-derived suppressor cells in cancer immunotherapy, Cancers 12 (2020) 2626.

Figure legends

Figure 1. Preferential accumulation of MO-MDSCs in tumor draining lymph nodes.
(A) Representative Ly6G vs Ly6C flow cytometry stainings on gated $CD11b^+$ cells from the SPL, cLNs and tdLNs of EG7-OVA tumor-bearing (TB) mice and the calculation of the ratio of MO-/PMN-MDSC for each organ are illustrated. **(B)** Absolute number of MO- and PMN-MDSCs in the different organs of naïve and EG7-OVA TB mice. The average volume of the EG7-OVA tumors, used in **A** and **B**, was 1436,5±312,4 mm^3. **(C)** MO-/PMN-MDSCs ratio and **(D)** absolute numbers of MO- and PMN-MDSCs in cLNs and tdLNs of EG7-OVA TB splenectomized mice as compared to EG7-OVA TB sham operated mice. Bars represent the mean +/- SEM of 6 individual replicates, tested in 2 independent experiments. The average volume of the EG7-OVA tumors, used in **C** and **D**, was 1285,3±251,6 mm^3 for the splenectomized mice and 1346,9±217,6 mm^3 for the sham operated mice **(E)** Percentage suppression of OT-I $CD8^+$ T-cell proliferation and **(F)** the concentration of NO present in the supernatant are measured 42h after coculture of various ratios of EG7-OVA TB mice-derived MO-MDSC (from tdLN or SPL) with ovalbumin-stimulated splenocytes from OT-I TCR transgenic mice. Bars represent the mean ± SEM of at least 9 individual replicates, tested in 4 independent experiments. *$p<0.05$; **$p<0.01$, ns: not significant (Wilcoxon matched pairs test).

Figure 2. Enhanced migration of MO-MDSCs, but not PMN-MDSCs, to tumor-draining lymph nodes.
(A) BrdU incorporation by MO- or PMN-MDSCs in SPL, cLNs and tdLNs was determined by flow cytometry. The percentage $BrdU^+$ cells is indicated. The average volume of the EG7-OVA tumors was 1311,1±183,2 mm^3. **(B)** Scheme of the MDSC adoptive transfer experiment. **(C)** Representative Ly6C vs Ly6G stainings of pre-gated $CD11b^+GFP^+$ cells (identifying MO- and PMN-MDSC) before (D0) and 16 h after (D1) transfer into naïve or 20-days EG7-OVA TB recipients. **(D)** MO-/PMN-MDSC ratio among GFP^+CD11b^+ cells before transfer (D0) and in SPL, cLNs and tdLNs of 20-days TB mice or SPL, cLN of naïve mice 16 h after transfer (D1). The average volume of the EG7-OVA tumors was

1449,0±332,7 mm^3. Bars represent the mean ± SEM of at least 8 individual replicates, tested in 7 independent experiments. *p<0.05, **p<0.01, ***p<0.001, ns: not significant (Mann-Whitney test).

Figure 3. Preferential accumulation of MO-MDSCs in tumor draining lymph nodes is not driven by metastasis at this site.

(A) Representative Ly6G vs Ly6C flow cytometry staining on gated $CD11b^+$ cells from 21-days EG7-OVA primary tumors. The mean ratio of MO-/PMN-MDSC is shown. The same TB mice were used as in Figure 1A-B. **(B)** Total RNA was isolated from the primary tumor (EG7 Tum), cLN and tdLN of 10-days TB mice or from LN of naïve mice for qRT-PCR analysis of ovalbumin (OVA) mRNA. OVA mRNA expression is shown relative to the expression of the S12 housekeeping gene. Data are shown as mean of n=4. **(C)** The ratio of MO-/PMN-MDSC was calculated for each organ from 10-days TB mice. **(D)** Absolute number of MO- and PMN-MDSCs in the different organs of 10-days TB mice. The average volume of the EG7-OVA tumors, used in **B-D** was 249,1±60,8 mm^3. **(E)** MO-/PMN-MDSC ratio among GFP^+CD11b^+ cells before transfer (D0) and in SPL, cLN and tdLNs of 10-days TB mice or SPL, cLN of naïve mice 16h after the adoptive transfer (D1). The average volume of the EG7-OVA tumors was 227,3±48,8 mm^3. Bars represent the mean ± SEM of at least 8 individual replicates, tested in 3 independent experiments. *p<0.05, **p<0.005, ns: not significant (Wilcoxon matched pairs test).

Figure 4. Homing of MO-MDSCs, but not PMN-MDSCs, to tumor-draining lymph nodes is CCR2-mediated.

(A) Expression of the chemokine receptors CCR2 and CCR7 by MO- and PMN-MDSCs from SPL, cLNs and tdLNs of EG7-OVA TB mice was analyzed via FACS. MO- and PMN-MDSCs were gated according to Supplementary Figure 1. Representative histograms from one mouse out of at least 4 individual replicates, tested in 3 independent experiments, are shown. **(B)** CCL2 production was measured by ELISA upon lysis of LN of either naïve or EG7-OVA TB mice or lysis of tumor tissue of TB mice 21 days (D21) after cancer cell inoculation. The average volume of the EG7-OVA tumors was 1095,3±195,6 mm^3. **(C)** Absolute number of MO- and PMN-MDSCs in SPL, cLNs and tdLNs of WT or $CCR2^{-/-}$ 21-days TB mice. The average volume of the EG7-OVA tumors was 1389,3±278,7 mm^3 in WT

mice, and 1137,4±156,5 mm^3 in $CCR2^{-/-}$ mice. **(D) Upper panel**: Scheme of the MDSC adoptive transfer experiment. **Lower panels:** Representative FACS plots of the percentage of WT (GFP^+) and $CCR2^{-/-}$ (GFP^-) cells within the transferred $CD45.1^-CD45.2^+Ly6C^{hi}$ MO-MDSCs or $CD45.1^-CD45.2^+Ly6G^+$ PMN-MDSCs in cLNs and tdLNs of naïve and TB mice (left panel). Percentage of WT (GFP^+) and $CCR2^{-/-}$ (GFP^-) cells among the transferred $Ly6C^{hi}$ (MO-MDSC) and $Ly6G^+$ (PMN-MDSC) populations (right panel). Bars represent the mean ± SEM of 3 independent experiments, each comprising 3 replicates. *$p<0.05$ (Mann-Whitney test).

Figure 1

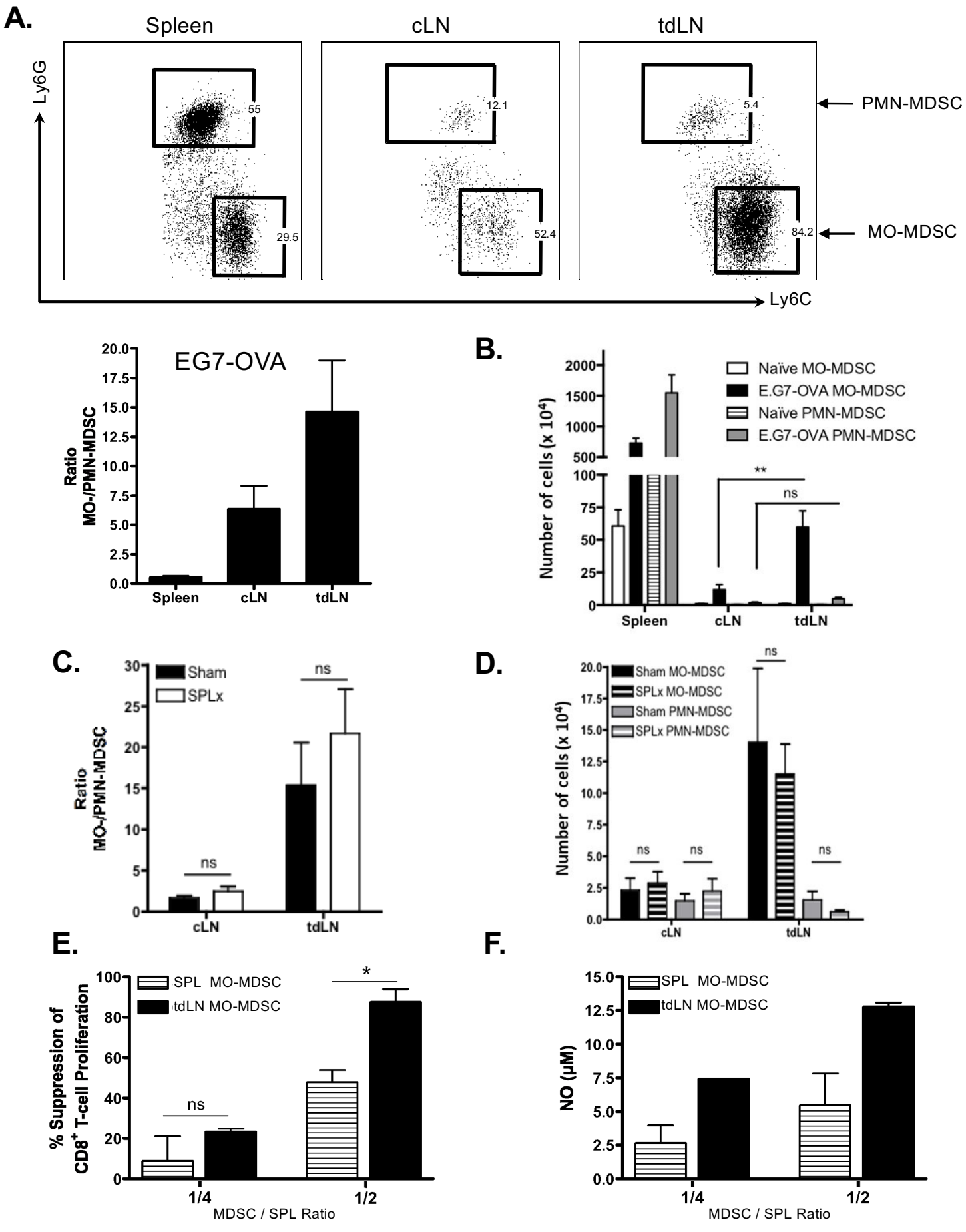
A.
Spleen
cLN
tdLN
Ly6G
Ly6C
55
29.5
12.1
52.4
5.4
84.2
PMN-MDSC
MO-MDSC
EG7-OVA
Ratio MO-/PMN-MDSC
Spleen
cLN
tdLN
B.
Naïve MO-MDSC
E.G7-OVA MO-MDSC
Naïve PMN-MDSC
E.G7-OVA PMN-MDSC
Number of cells (x 10⁴)
**
ns
C.
Sham
SPLx
Ratio MO-/PMN-MDSC
ns
D.
Sham MO-MDSC
SPLx MO-MDSC
Sham PMN-MDSC
SPLx PMN-MDSC
Number of cells (x 10⁴)
E.
SPL MO-MDSC
tdLN MO-MDSC
% Suppression of CD8⁺ T-cell Proliferation
*
1/4
1/2
MDSC / SPL Ratio
F.
SPL MO-MDSC
tdLN MO-MDSC
NO (μM)
MDSC / SPL Ratio

Figure 2

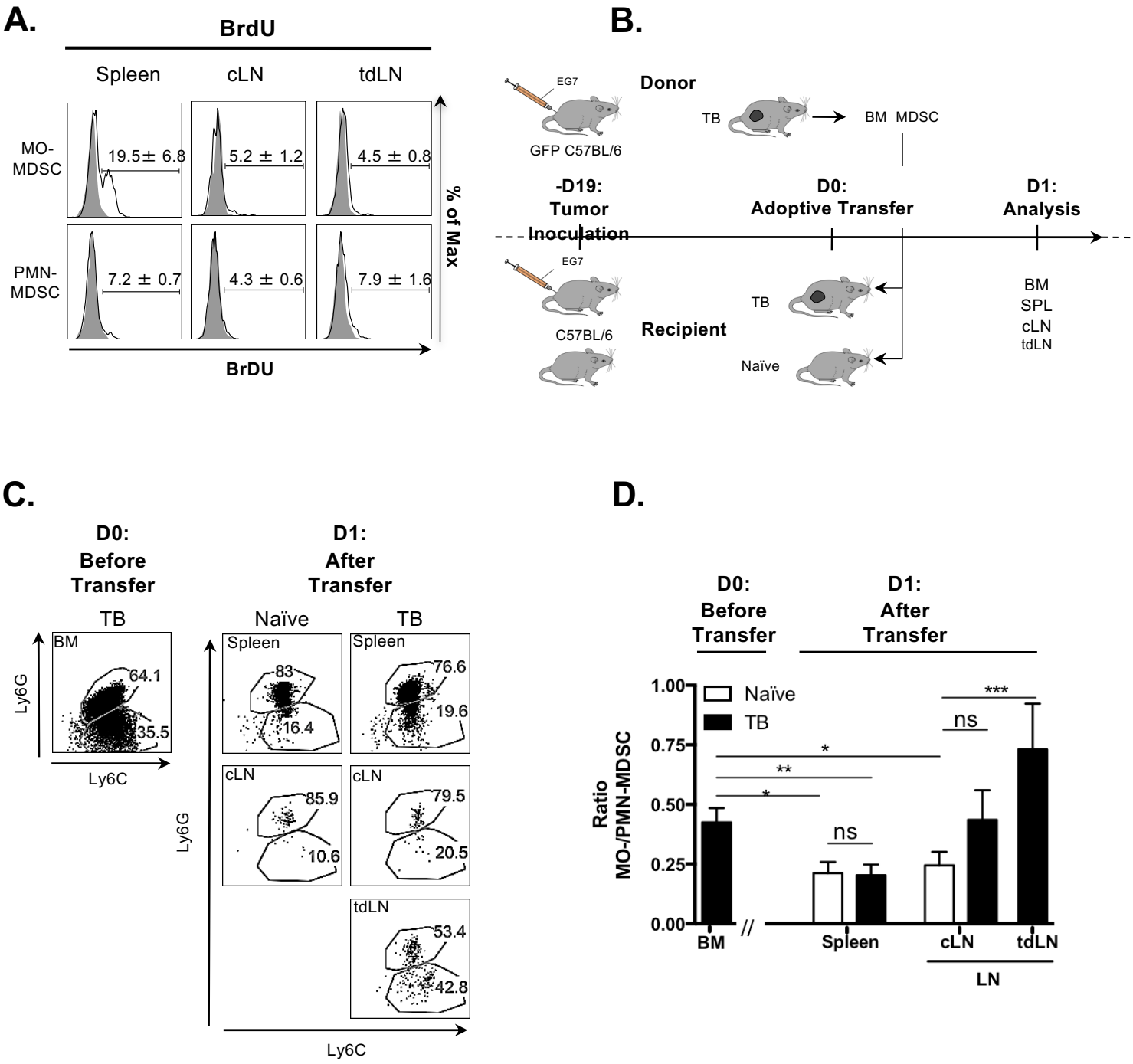
A.
BrdU
Spleen
cLN
tdLN
MO-MDSC
PMN-MDSC
19.5± 6.8
5.2 ± 1.2
4.5 ± 0.8
7.2 ± 0.7
4.3 ± 0.6
7.9 ± 1.6
% of Max
BrDU
B.
EG7
GFP C57BL/6
Donor
TB
BM MDSC
-D19: Tumor Inoculation
D0: Adoptive Transfer
D1: Analysis
EG7
C57BL/6
Recipient
TB
Naïve
BM
SPL
cLN
tdLN
C.
D0: Before Transfer
D1: After Transfer
TB
Naïve
TB
BM
64.1
35.5
Spleen
83
16.4
Spleen
76.6
19.6
cLN
85.9
10.6
cLN
79.5
20.5
tdLN
53.4
42.8
Ly6G
Ly6C
Ly6G
Ly6C
D.
D0: Before Transfer
D1: After Transfer
Naïve
TB
Ratio MO-/PMN-MDSC
1.00
0.75
0.50
0.25
0.00
*
**
*
ns
ns
***
BM
Spleen
cLN
tdLN
LN

Figure 3

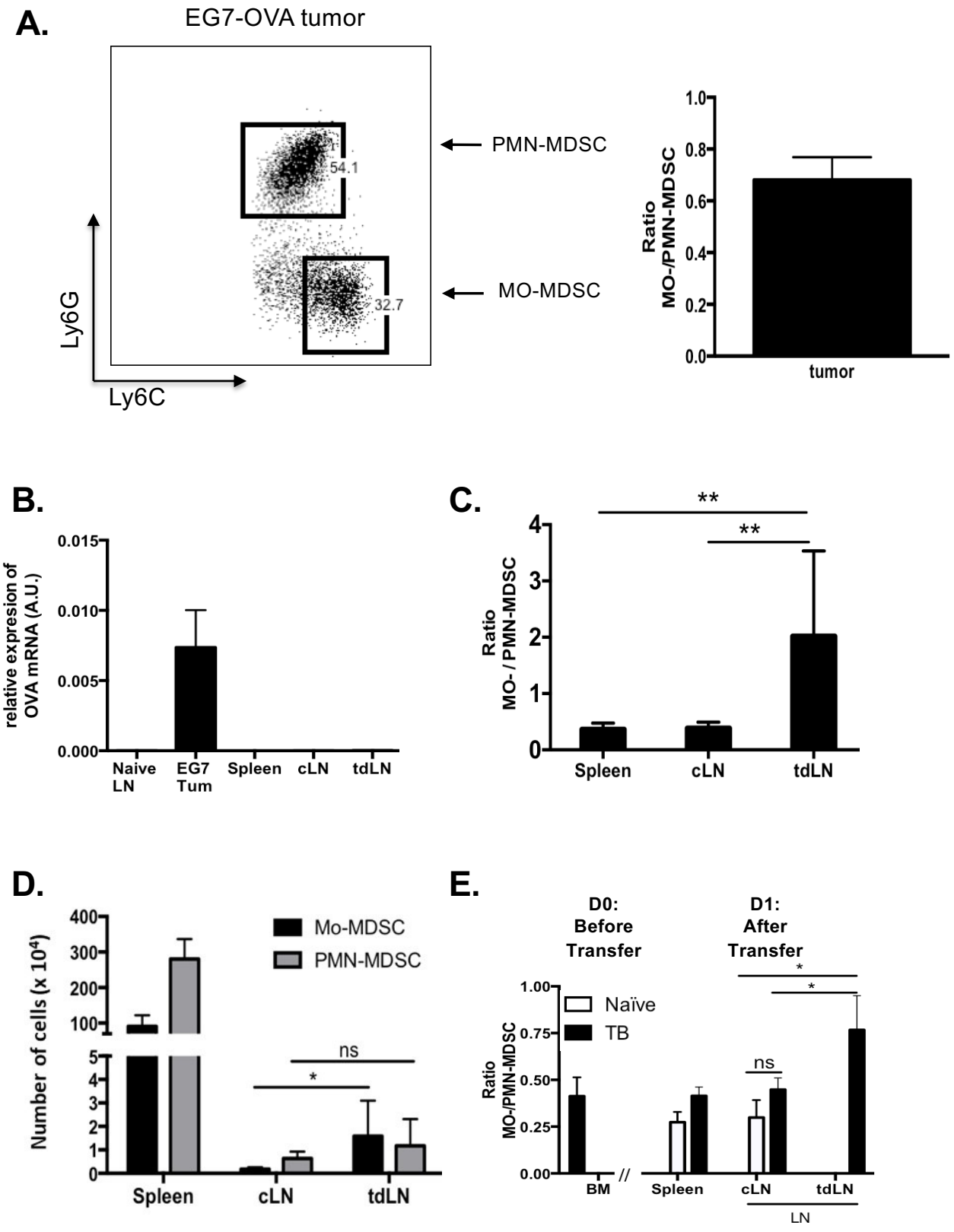
A.
EG7-OVA tumor
54.1
32.7
PMN-MDSC
MO-MDSC
Ly6G
Ly6C
Ratio MO-/PMN-MDSC
tumor
B.
relative expresion of OVA mRNA (A.U.)
Naive LN
EG7 Tum
Spleen
cLN
tdLN
C.
Ratio MO- / PMN-MDSC
**
**
Spleen
cLN
tdLN
D.
Number of cells (x 10⁴)
Mo-MDSC
PMN-MDSC
ns
*
Spleen
cLN
tdLN
E.
D0: Before Transfer
D1: After Transfer
Naïve
TB
Ratio MO-/PMN-MDSC
BM
Spleen
cLN
tdLN
LN
ns
*
*

Figure 4

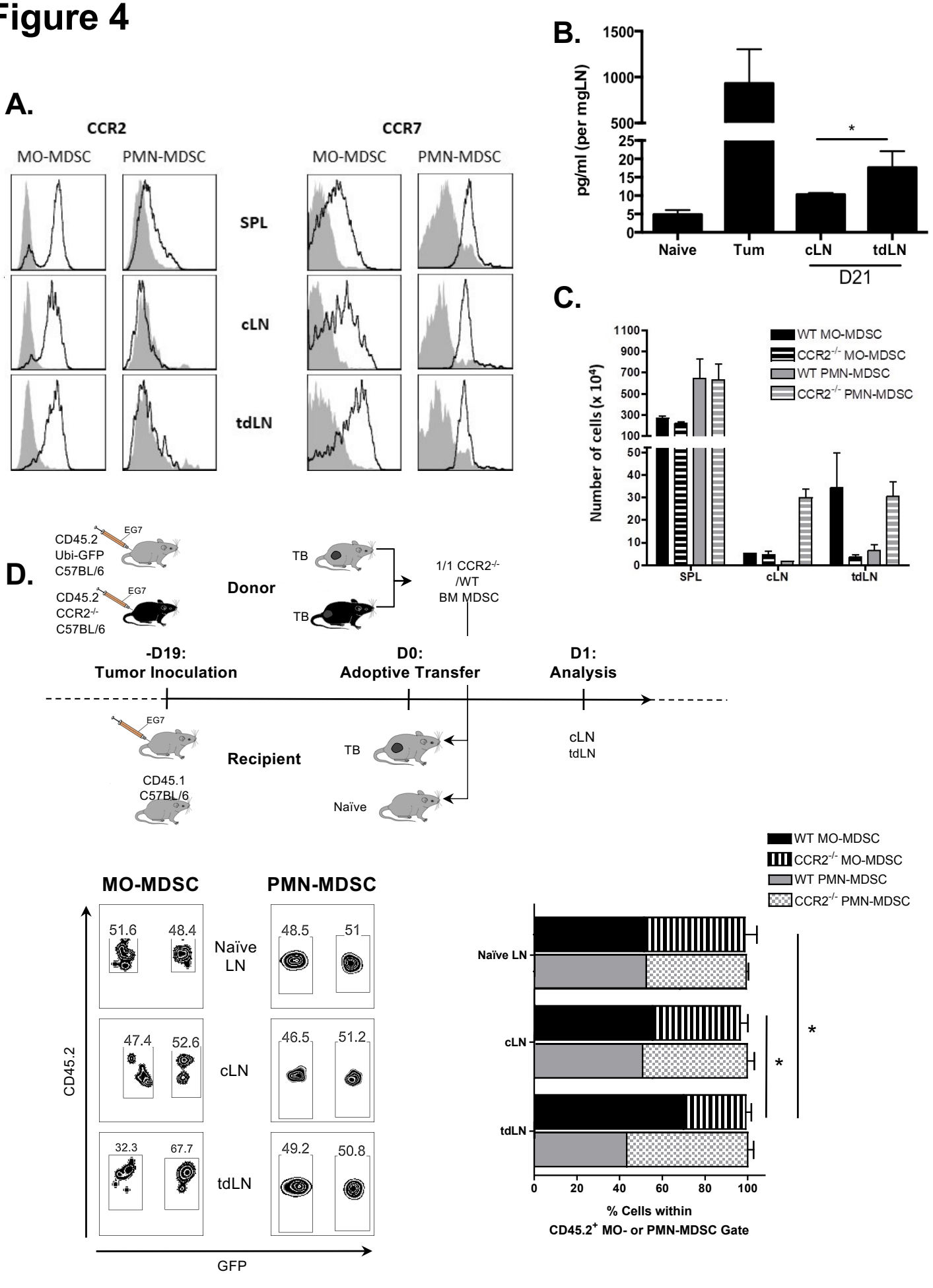
A.
CCR2
CCR7
MO-MDSC
PMN-MDSC
MO-MDSC
PMN-MDSC
SPL
cLN
tdLN
B.
pg/ml (per mgLN)
1500
1000
500
25
20
15
10
5
0
*
Naive
Tum
cLN
tdLN
D21
C.
Number of cells (x 10⁴)
1100
900
700
500
300
100
50
40
30
20
10
0
WT MO-MDSC
CCR2-/- MO-MDSC
WT PMN-MDSC
CCR2-/- PMN-MDSC
SPL
cLN
tdLN
D.
CD45.2
Ubi-GFP
C57BL/6
EG7
CD45.2
CCR2-/-
C57BL/6
EG7
Donor
TB
TB
1/1 CCR2-/-
/WT
BM MDSC
-D19:
Tumor Inoculation
D0:
Adoptive Transfer
D1:
Analysis
EG7
CD45.1
C57BL/6
Recipient
TB
Naïve
cLN
tdLN
MO-MDSC
PMN-MDSC
51.6
48.4
48.5
51
Naïve
LN
47.4
52.6
46.5
51.2
cLN
32.3
67.7
49.2
50.8
tdLN
CD45.2
GFP
WT MO-MDSC
CCR2-/- MO-MDSC
WT PMN-MDSC
CCR2-/- PMN-MDSC
Naïve LN
cLN
tdLN
*
*
0
20
40
60
80
100
% Cells within
CD45.2+ MO- or PMN-MDSC Gate

Supplementary Table 1

List of antibodies.

Marker	Clone	Manufacturer
CD11b	M1/70	BD Bioscience
CCR7	4b12	eBioscience
CD11c	HL3	BD Bioscience
CD19	30-H12	BD Bioscience
Ki67	B56	BD Bioscience
Ly6G	1A8	BD Bioscience
F4/80	A3-1	AbD Serotec
Ly6C	ER-MP20	AbD Serotec
CCR2	475301	R&D sytstems
MHC II	M5/114.15.2	Biolegend
CD16/CD32	2.4G2	BD Bioscience

Supplementary Table 2

List of gene specific primers.

Gene	Forward Primer	Reverse Primer
S12	GGAAGGCATAGCTGCTGGAGGTGT	CCTCGATGACATCCTTGGCCTGAG
OVA	CGTGGATTCTCAAACTGCAA	CACCAACATGCTCATTGTCC
CCL2	CACTCACCTGCTGCTACTCATTCAC	GGATTCACAGAGAGGGAAAAATGG

Supplementary figure 1

MDSC gating strategy

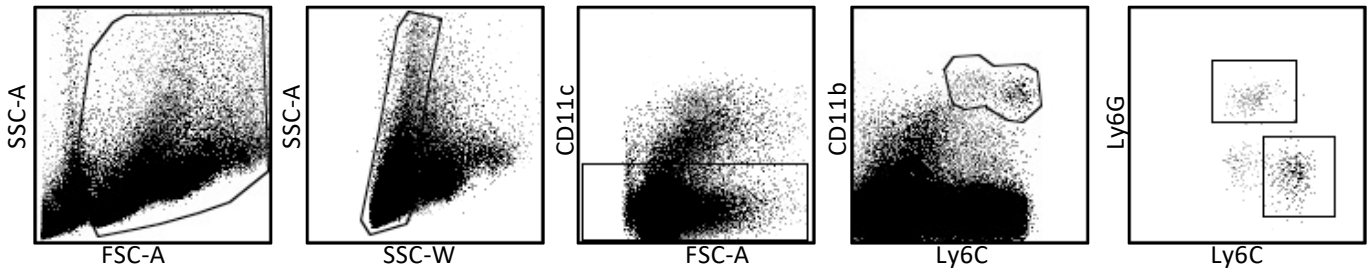

Supplementary Figure 1. Gating strategy for MDSCs

Gating strategy for MDSC subsets in spleen and lymph nodes. Viable Singlet CD11c- cells were examined for their CD11b and Ly6C expression. $Cd11b^{+}Ly6C^{+}$ cells were gated into $Ly6G^{+}Ly6C^{int}$ PMN-MDSCs and $Ly6G^{-}Ly6C^{high}$ MO-MDSCs.

Supplementary figure 2

A. 3LL-R

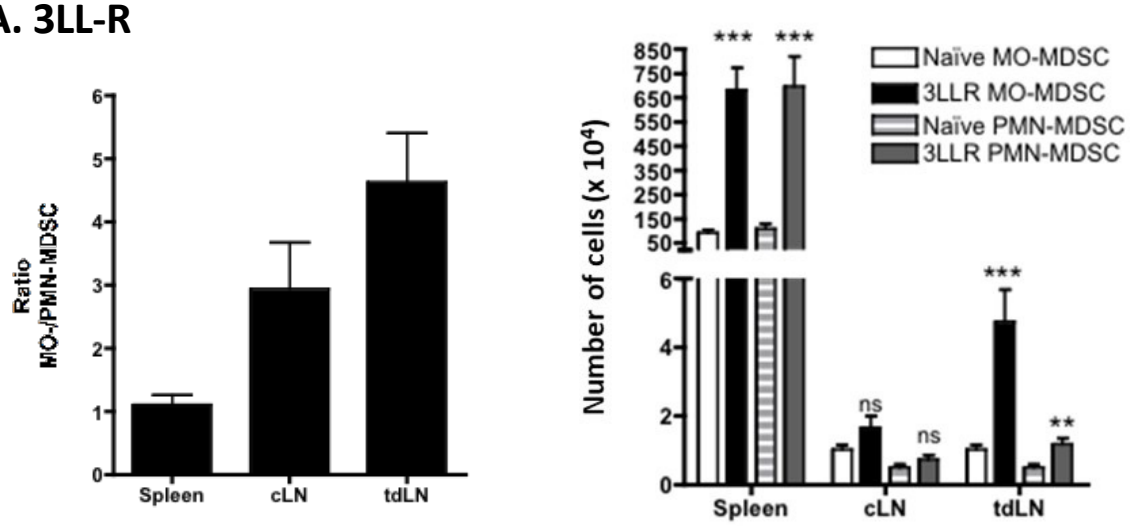

B. E0771

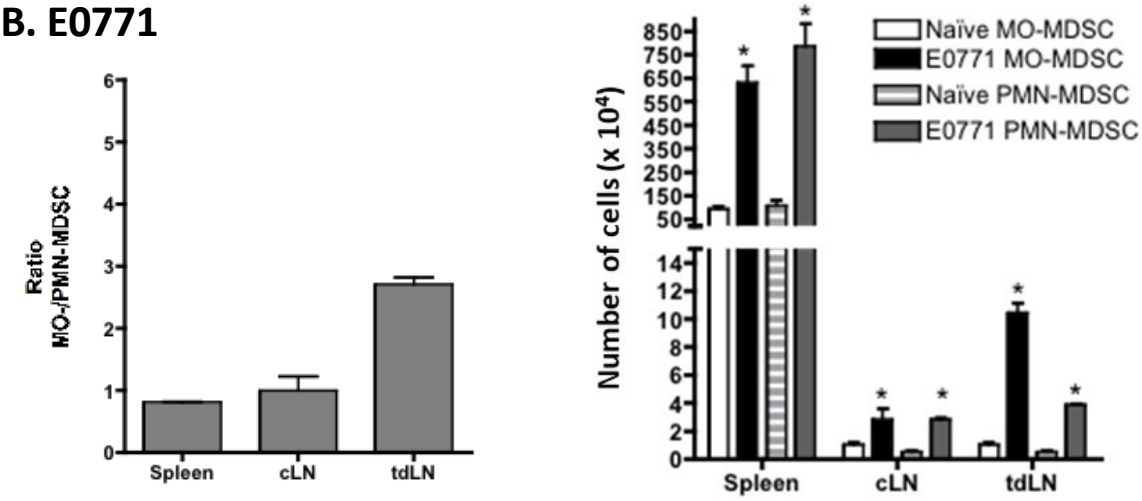

Supplementary Figure 2. Preferential accumulation of MO-MDSCs in the tumor-draining LNs of 3LL-R and E0771 tumor bearing mice

MO-/PMN-MDSCs ratio and absolute numbers of MDSCs in SPL, cLNs and tdLNs of (A) 3LL-R (average tumor volume 1946,4±402,1 mm^3) and (B) E0771 (average tumor volume 1139,8±267,0 mm^3) TB mice as compared to naïve mice. Bars represent the mean +/- SEM of at least 4 individual replicates, tested in 2 independent experiments.

Supplementary figure 3

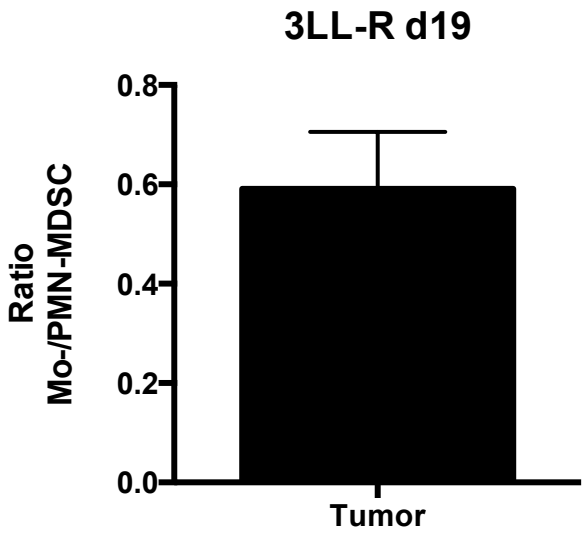

Supplementary Figure 3. MO-/PMN-MDSC ratio in 3LL-R tumors.

MO-/PMN-MDSCs ratio in a single cell suspension of 19 day-old 3LL-R tumors (average tumor volume as in Suppl Figure 2). Bars represent the mean +/- SEM of at least 4 individual replicates, tested in 2 independent experiments.

Supplementary figure 4

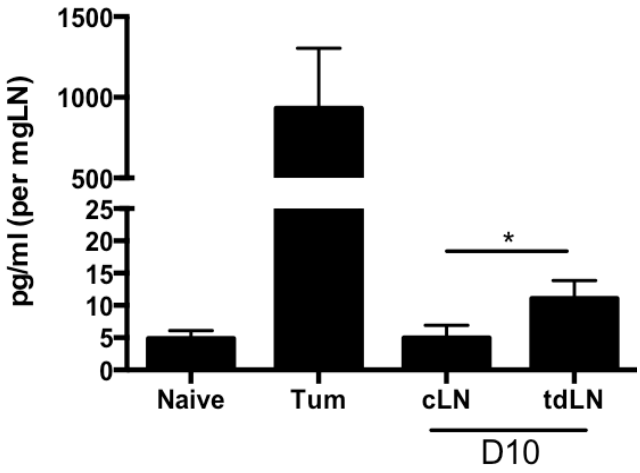

Supplementary Figure 4. Presence of CCL2 protein in LN from day 10 EG7-OVA tumor-bearing mice.

CCL2 production was measured by ELISA upon lysis of LN of either naïve or EG7-OVA (average tumor volume 193,4±81,9 mm^3) TB mice or lysis of tumor tissue of TB mice 10 days (D10) after cancer cell inoculation, and expressed per mg LN tissue.

Supplementary figure 5

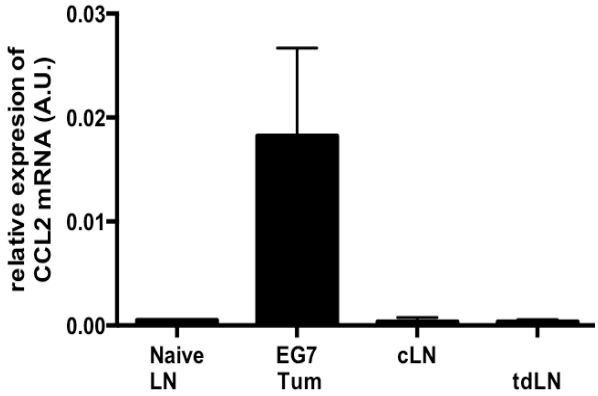

Supplementary Figure 5. Lack of *Ccl2* mRNA expression in cLN and tdLN of EG7-OVA tumor-bearing mice.

CCL2 mRNA levels were measured by qRT-PCR in naïve LN, tumor tissue (EG7 Tum), cLN and tdLNs of 21-days EG7-OVA bearing mice (average tumor volume as in Figure 4B). *Ccl2* mRNA expression is shown relative to the expression of the S12 housekeeping gene.